symmetry

MDPI

*Article*

# A Class of Discrete Memristor Chaotic Maps Based on the Internal Perturbation

**Worke Adugna Yihyis [1], Shaobo He [2], Zhouqing Tang [1] and Huihai Wang [1,*]**

[1] School of Electronic Information, Central South University, Changsha 410083, China
[2] School of Automation and Electronic Information, Xiangtan University, Xiangtan 411105, China
* Correspondence: wanghuihai_csu@csu.edu.cn

**Abstract:** Further exploration into the influence of a memristor on the behavior of chaotic systems deserves attention. When constructing memristor chaotic systems, it is commonly believed that increasing the number of memristors will lead to better system performance. This paper proposes a class of chaotic maps with different discrete memristors, achieved through internal perturbation based on the Sine map. The I-V curve of the discrete memristor has a symmetrical structure. The dynamic characteristics of the designed system are analyzed using the chaotic attractor phase diagram, Lyapunov exponent (LE) spectrum, and bifurcation diagram. Numerical simulations demonstrate that internal perturbations of discrete memristors enhance the Sine map's chaotic characteristics, expand the chaos range, and improve the ergodicity and LE value. Moreover, the type of discrete memristors has a significant impact on the dynamic characteristics of the system, while the number of discrete memristors has little influence. Therefore, in this paper, a direction for the design of a discrete memristor chaotic system is provided. Finally, a discrete memristor chaotic map with a simple structure and better performance is selected. Based on this, a pseudo-random sequence generator is designed, and the generated sequence passes the National Institute of Standards and Technology (NIST) test.

**Keywords:** chaos; discrete memristor; internal perturbation; Sine map; symmetry



**Citation:** Yihyis, W.A.; He, S.; Tang, Z.; Wang, H. A Class of Discrete Memristor Chaotic Maps Based on the Internal Perturbation. *Symmetry* **2023**, *15*, 1574. https://doi.org/10.3390/sym15081574

Academic Editor: Wiesław Leonski

Received: 18 June 2023
Revised: 31 July 2023
Accepted: 3 August 2023
Published: 12 August 2023



## 1. Introduction

The memristor, first proposed by Prof. Chua [1] in 1971, was identified as the fourth essential component of a circuit, after resistors, inductors, and capacitors. Later, in 1976, Chua and Kang [2] explored this concept as a generalized memristor. In 2008, HP Laboratory demonstrated that a nanoscale $TiO_2$ device was a real memristor [3]. In 2013, Adhikari et al. [4] proposed the three fingerprint features that guided the design of generalized memristors. Since then, researchers have become increasingly interested in exploring memristors and applying them to various fields, such as nanotechnology [5], neural networks [6–9], circuit design [10], image encryption [11–13], secure communication [14], and so on. In addition, memristors have the potential to revolutionize data storage by providing faster access times, higher storage densities, and lower power consumption compared to traditional solid-state drives. In 2021 [15], the super track method was applied, for the first time, to an electric circuit, particularly Chua's circuit with a memristor. The researcher utilizes both analytical and numerical techniques to explore the realistic model in coupled identical memristor-based Chua's circuit [16].

Recently, some scholars and researchers have focused on chaotic systems with memristors [17–20]. A chaotic system is a non-linear dynamic system that moves in a seemingly random and irregular motion, and it has been utilized frequently in information security areas because of its initial sensitivity value and unpredictability [21,22]. Memristors are commonly used to build nonlinear systems that exhibit complex dynamical behavior. Many researchers have shown the dynamic phenomena of the chaotic system with memristors, such as multistability, transient phenomena, bi-stability, symmetry, and dissipation [23–25].

It is worth noting that memristors can generate chaos and increase the complexity of chaos, opening up a new line of research for chaos design and improvement [26]. Numerous theoretical and experimental studies concerning the application of a continuous memristor in a chaotic system have been discussed in [27–29]. In 2020, He et al. [30] proposed a mathematical model for discrete memristors based on a different theory. Like a continuous memristor, the discrete memristor has a symmetric I-V curve. However, discrete memristors are better suited for discrete chaotic maps and digital circuits, and they can easily be implemented by hardware circuits. Moreover, discrete chaotic maps are easy to replicate, which is beneficial for their application. Therefore, the researchers introduced discrete memristors to construct different chaotic maps, and the advantage of discrete memristors in chaotic systems has grown significantly [31,32]. Liu et al. [33] introduced discrete memristors to a chaotic map by coupling with trigonometric functions, which performed the coexistence of multiple chaotic and hyperchaotic attractors. Peng et al. [34] established three fractional-order discrete memristor chaotic maps based on Caputo's fractional-order difference and analyzed the dynamic behaviors of the systems with different models. Li et al. [35] designed the Simulink model of the discrete memristor chaotic system to enhance its chaotic behavior. Ma et al. [36] analyzed the characteristics of coupled memristor chaotic maps in non-fixed points. Ren et al. [37] constructed a new three-dimensional hyperchaotic map by coupling the discrete memristor, providing the application of discrete memristor circuits in chaotic systems. The preceding research studies demonstrate that discrete memristor models can enhance the dynamic behaviors of chaotic systems.

In many instances of chaotic system construction in research studies, researchers have chosen the sine function as the seed because it is one of the simplest chaotic maps. Sun et al. [38], based on the Sine map, proposed a memristive seed chaotic map by a quadratic memristor combination that can generate hyperchaos. Hua et al. [39] proposed the chaotification model for enhancing the chaos complexity of the system on the Sine map, and Li et al. [40] investigated the fractional difference form of this model to improve its chaotic behavior. Dong et al. [41] focused on constructing and modulating a high-dimensional chaotic system using a Sine map, but they did not consider the impact of the type and quantity of discrete memristors on the Sine map system as its internal perturbation model. Building upon their work, we incorporate a discrete memristor into the Sine map to create an internal perturbation model. Additionally, we investigate how the type and number of discrete memristors affect the system's performance. It is important to note that the complexity of the chaotic system is not solely determined by the quantity of memristors used, but rather by the specific type of memristor employed. In this paper, we select a discrete memristor chaos model with a simple structure and enhanced performance for the application. These offer valuable guidance for designing discrete memristor chaotic systems.

The remainder of this paper is organized as follows: Section 2 describes a discrete memristor and proposes internal perturbation models. In Section 3, the single discrete memristor perturbation models are analyzed. In Section 4, the multiple discrete memristor perturbation models are studied. In Section 5, a pseudo-random sequence generator is designed based on a simple and superior discrete memristor perturbation model. The conclusion is presented in Section 6.

## 2. Design of a Memristor Model with Internal Perturbation

### *2.1. The Discrete Memristor*

Based on existing continuous memristors [42] and difference theories, four mathematical representations of discrete memristors are deduced. The discrete memristors include the quadratic discrete memristor (Q-DM), absolute value discrete memristor (A-DM), sinusoidal discrete memristor (S-DM), and exponential discrete memristor (E-DM). The mathematical expressions of these four discrete memristors are described as follows [43]:

$$M(q_n) = q_n^2 - 1 \tag{1}$$

$$M(q_n) = |q_n| - 1 \tag{2}$$

$$M(q_n) = \sin(\pi q_n) + c \tag{3}$$

$$M(q_n) = e^{-\cos(\pi q_n)} - 1 \tag{4}$$

where $c$ is a parameter, $M(q_n)$ represents the memristance of the discrete memristor, and $q_n$ is the charge contained in discrete memristors at the $n$-th iteration. According to Ohmś law and the forward Euler difference algorithm, the relationship between the voltage $V_n$ and current ($i_n$) at both ends of a discrete memristor is shown in Equation (5) [44].

$$\begin{cases} V_n = M(q_n) i_n \\ q_{(n+1)} = q_n + i_n \end{cases}, \tag{5}$$

where $V_n$ and $i_n$ are the sample of output $v(t)$ and input $i(t)$ at the $n$-th iteration, respectively. In discrete memristors, the charge amount that passes through the component is measured at specific intervals or iterations. Setting $q_0 = 0$, a bipolar periodic sinusoidal current signal $i_n = 0.01 \sin\ (\omega\pi)$ with variable frequencies passes through the discrete memristors. The voltage and current planes of the Q-DM, A-DM, S-DM, and E-DM are plotted in Figure 1, where $c = 0.5$ is for S-DM. As shown in Figure 1, the four discrete memristors all match the three fingerprint characteristics: (1) a hysteresis curve of the "∞" shape on the voltage and current planes; (2) a monotonic decrease in the area of the hysteresis curve beyond a certain critical frequency with an increase in excitation frequency; (3) the shrinking of the hysteresis curve to a single-valued function at infinity frequency $\omega$. The I-V curves of these four discrete memristors are symmetric around the origin. They are generalized memristors.

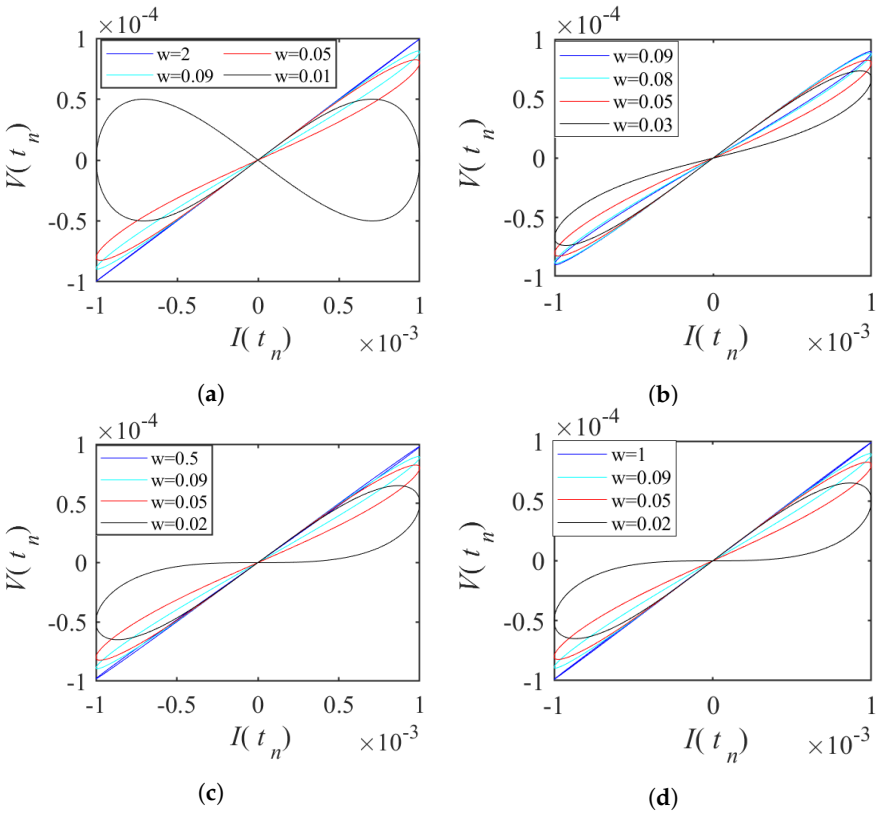


**Figure 1.** The hysteresis loop of the discrete memristor with different frequencies at $q_0 = 0$ (**a**) Q-DM, (**b**) A-DM, (**c**) S-DM, (**d**) E-DM.

### 2.2. The Sine Map

A Sine map is expressed in [45] as follows:

$$x_{n+1} = a \sin(\omega x_n) \tag{6}$$

where $a$ is the system parameter that is greater than zero. Figure 2 displays the chaotic attractor of the original Sine map at $a = 3.4, \omega = \pi$, $x_0 = 0.1$, and indicates that the system in a chaotic state exhibits low ergodicity. By varying $a$ from 0 to 4 with a step size of 0.02, the LE and bifurcation diagram of the Sine map are plotted in Figure 3. As shown in Figure 3a, the periodic windows and chaotic intervals appear alternately with varying system parameters $a$. In addition, Figure 3b shows that the LE value is smaller than 2 throughout the parameter range.

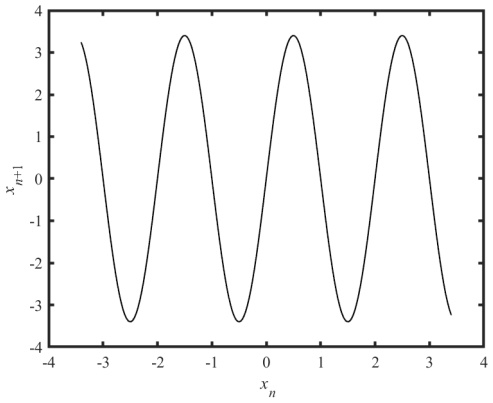


**Figure 2.** Chaotic attractor diagram of the Sine map at $a = 3.4$ and $\omega = \pi$.

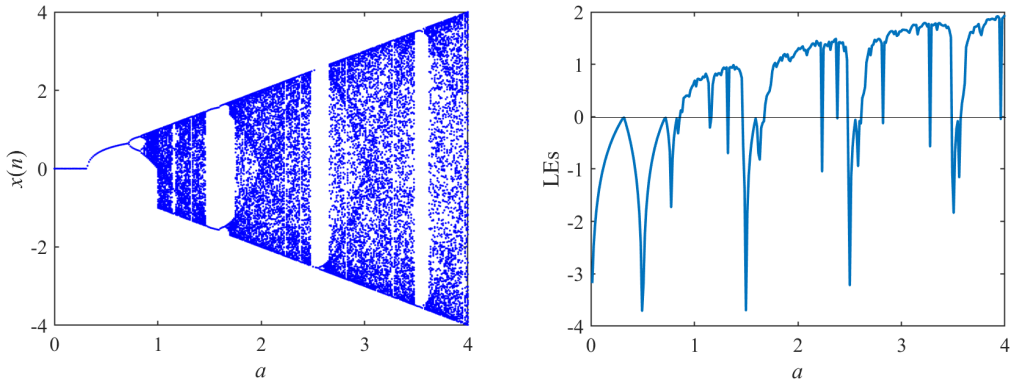


(**a**) (**b**)

**Figure 3.** (**a**) The bifurcation diagram of the Sine map, (**b**) the LEs of the Sine map.

### 2.3. Chaotic Maps with Discrete Memristor Perturbations

The proposed internal perturbation model (IPM) aims to enhance the chaotic complexity of the seed map. Figure 4 shows the block diagram structure of the IPM based on a discrete memristor with a single internal perturbation, where $D$ represents a unit delay. In this design, the Sine map serves as the basic map, while a discrete memristor is used as the perturbation. The memristor regulates the input of the Sine map, providing perturbation terms that generate and regulate the system. The equation of a single perturbation model is expressed as follows:

$$x_{n+1} = a \sin(\omega(x_n - bM(q_n)x_n)) \tag{7}$$

where $b$ is the control parameter of the discrete memristor, and $M(q_n)$ is a type of memristor.

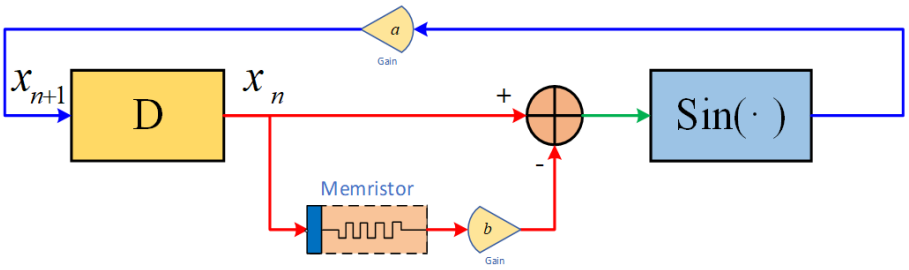


**Figure 4.** The block diagram of IPM with a single memristor.

In this study, we explore the impacts of the type and number of discrete memristors on the system performance. Therefore, an internal perturbation model with multiple discrete memristors is proposed by connecting memristors in parallel, which modulates the dynamics of a high-dimensional chaotic system. The block diagram of the proposed model is shown in Figure 5. Specifically, the system is modulated by $N$ discrete memristors, and each provides a different perturbation model. The general equation for the $N$ internal perturbation memristors is as follows:

$$x_{n+1} = a\sin(\omega(x_n - b\sum_{k=1}^{N} M_k(q_n)x_n)) \tag{8}$$

where $M_k(q_n)$ is a memristor with $k = 1, 2, 3, \cdots, N$.

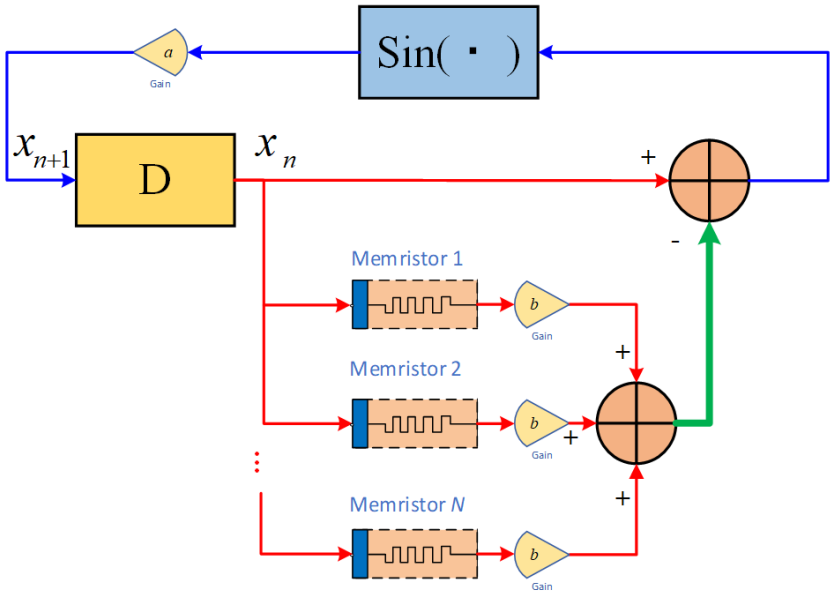


**Figure 5.** The block diagram of the internal perturbation model with multiple memristors.

## 3. Dynamics of the Sine Map with Single Internal Perturbation

In this section, IPM with a single perturbation is applied to the Sine map. To evaluate the effectiveness of the different discrete memristors in improving the dynamic behavior of the system, we add the different discrete memristors expressed by Equations (1)–(4). The block diagram of IPM with a single internal perturbation is displayed in Figure 4, based on this system diagram, applying Equation (7) as a single internal perturbation. The various single internal perturbation models are listed in Table 1. Based on these equations, chaotic attractor diagrams, bifurcation diagrams, and LE spectra for each model are analyzed.

**Table 1.** Multiple internal perturbation models of the memristor.

| Model | Memristor | Equation |
|---|---|---|
| Model 1 | Q-DM | $\begin{cases} x_{n+1} = a\sin(\omega(x_n - b(q_n^2 - 1)x_n)) \\ q_{n+1} = q_n + x_n \end{cases}$ |
| Model 2 | A-DM | $\begin{cases} x_{n+1} = a\sin(\omega(x_n - b(\lvert q_n\rvert - 1)x_n)) \\ q_{n+1} = q_n + x_n \end{cases}$ |
| Model 3 | S-DM | $\begin{cases} x_{n+1} = a\sin(\omega(x_n - b(\sin(\pi q_n) + c)x_n)) \\ q_{n+1} = q_n + x_n \end{cases}$ |
| Model 4 | E-DM | $\begin{cases} x_{n+1} = a\sin(\omega(x_n - b(e^{-\cos(\pi q_n)} - 1)x_n)) \\ q_{n+1} = q_n + x_n \end{cases}$ |

### *3.1. Chaotic Attractor of a Single Perturbation Model*

Here, we set the initial value $x_0 = 0.1, q_0 = 0.2$, step size $h = 0.02$, parameters $a = 3.4, b = 1, c = 0.5$, and $\omega = \pi$. Figure 6 displays the chaotic attractor diagram of the Sine map with four different single internal perturbation models. Compared with Figure 2, the original Sine map, the single internal perturbation models exhibit better ergodicity and more complex topology. Furthermore, as shown in Figure 6, different memristors have different effects on the shapes of the chaotic attractors. Model 1 and Model 2 demonstrate superior ergodicity than the other two models. To further investigate the impacts of different discrete memristors on the attractor phase diagram, we vary the value of the control parameter at $b = 1 \times 10^{-5}$. The chaotic attractor diagrams of the four corresponding models are shown in Figure 7. We can see that Model 1 has better ergodicity and a more complex topology compared to the other three models.

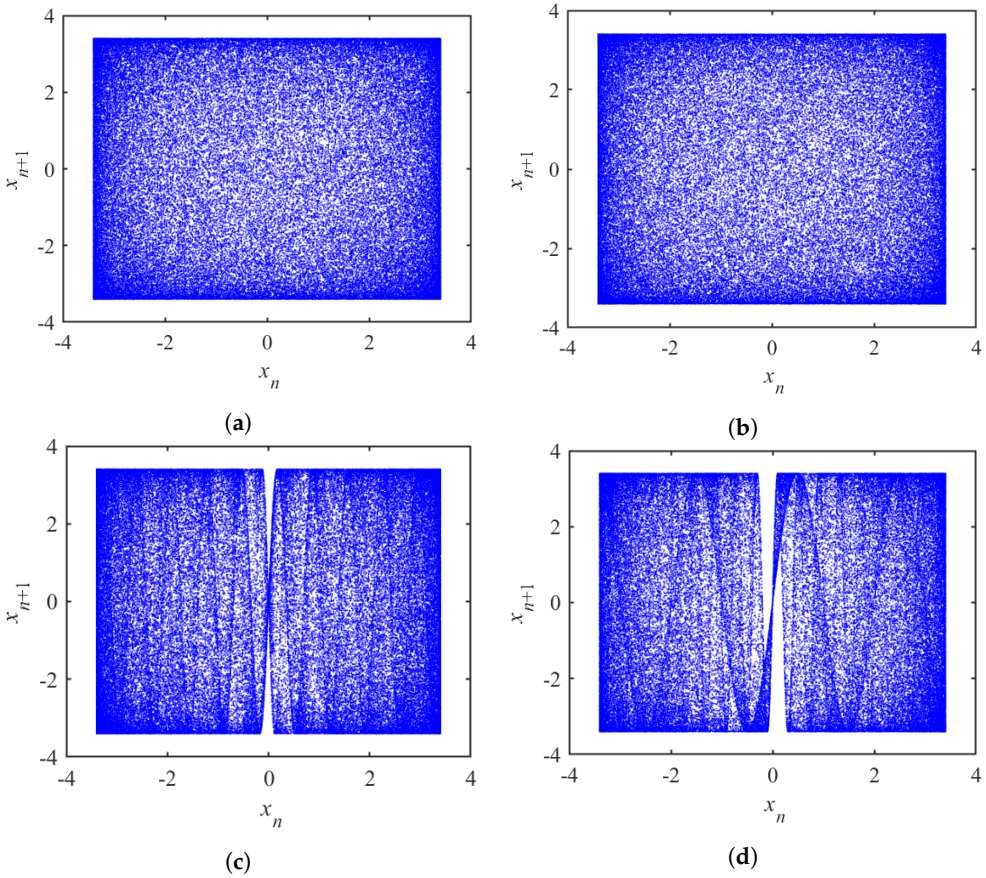


**Figure 6.** Chaotic attractors of a single perturbation with $a = 3.4$ and $b = 1$ (**a**) Model 1, (**b**) Model 2, (**c**) Model 3, (**d**) Model 4.

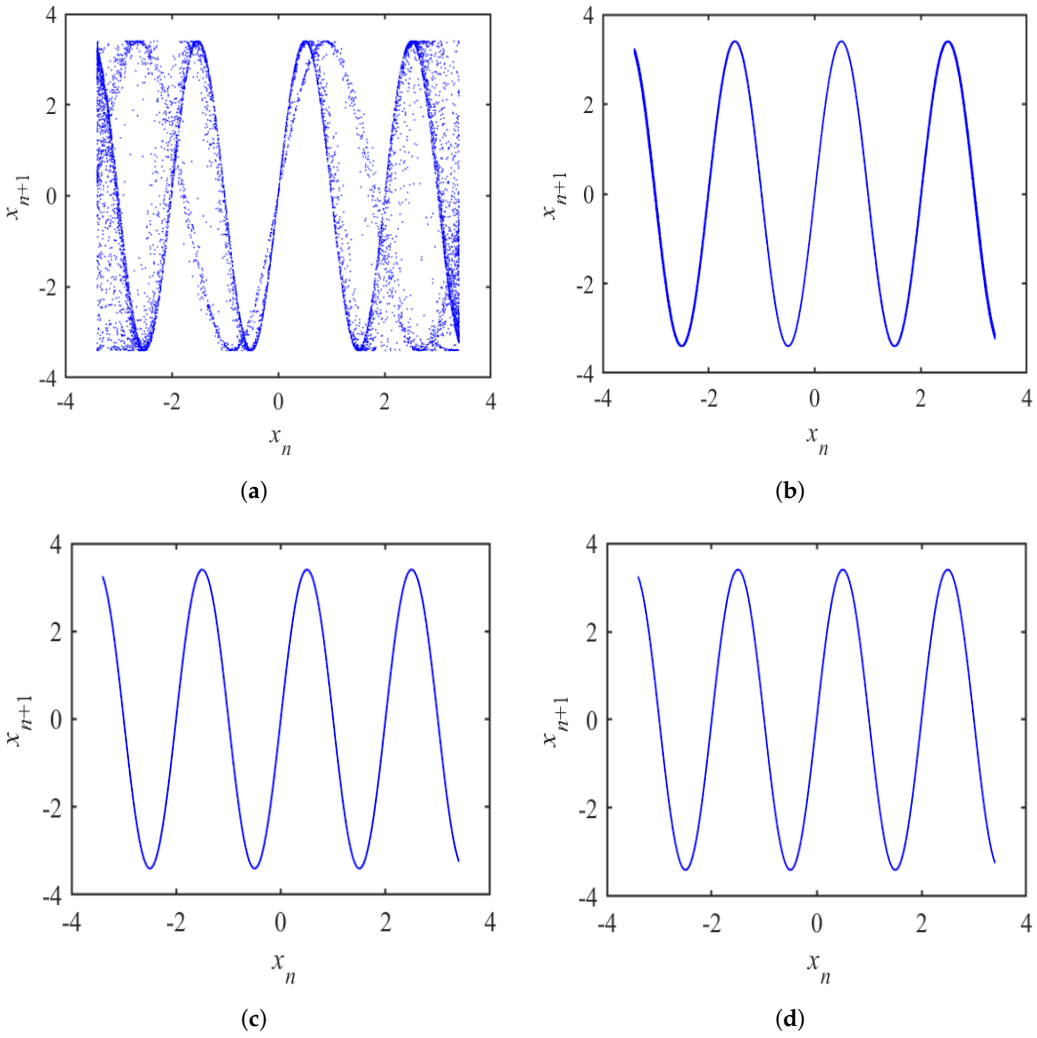


**Figure 7.** Chaotic attractors of a single perturbation with $a = 3.4$ and $b = 1 \times 10^{-5}$ (**a**) Model 1, (**b**) Model 2, (**c**) Model 3, (**d**) Model 4.

### *3.2. Bifurcation and LE of a Single Perturbation Model*

The LE is an important index to measure chaos. It represents the separation rate of adjacent trajectories in the phase space. The initial conditions are the same as those in Figure 6. The bifurcation diagram and LEs of the four models are exhibited in Figure 8. Compared with Figure 2, the single IPM has higher LE values and a wider range of chaos. The analysis shows that after the addition of a discrete memristor as an internal perturbation, the chaotic performance of the system is improved, as mainly reflected in the reduction of the period windows and the increase of the LE values. However, the degree of improvement in each model is different. It is obvious that among the four models, Model 1 has the largest LE value and the widest chaotic range, which indicates that the discrete memristor choice can significantly affect the dynamic behavior and complexity of the system.

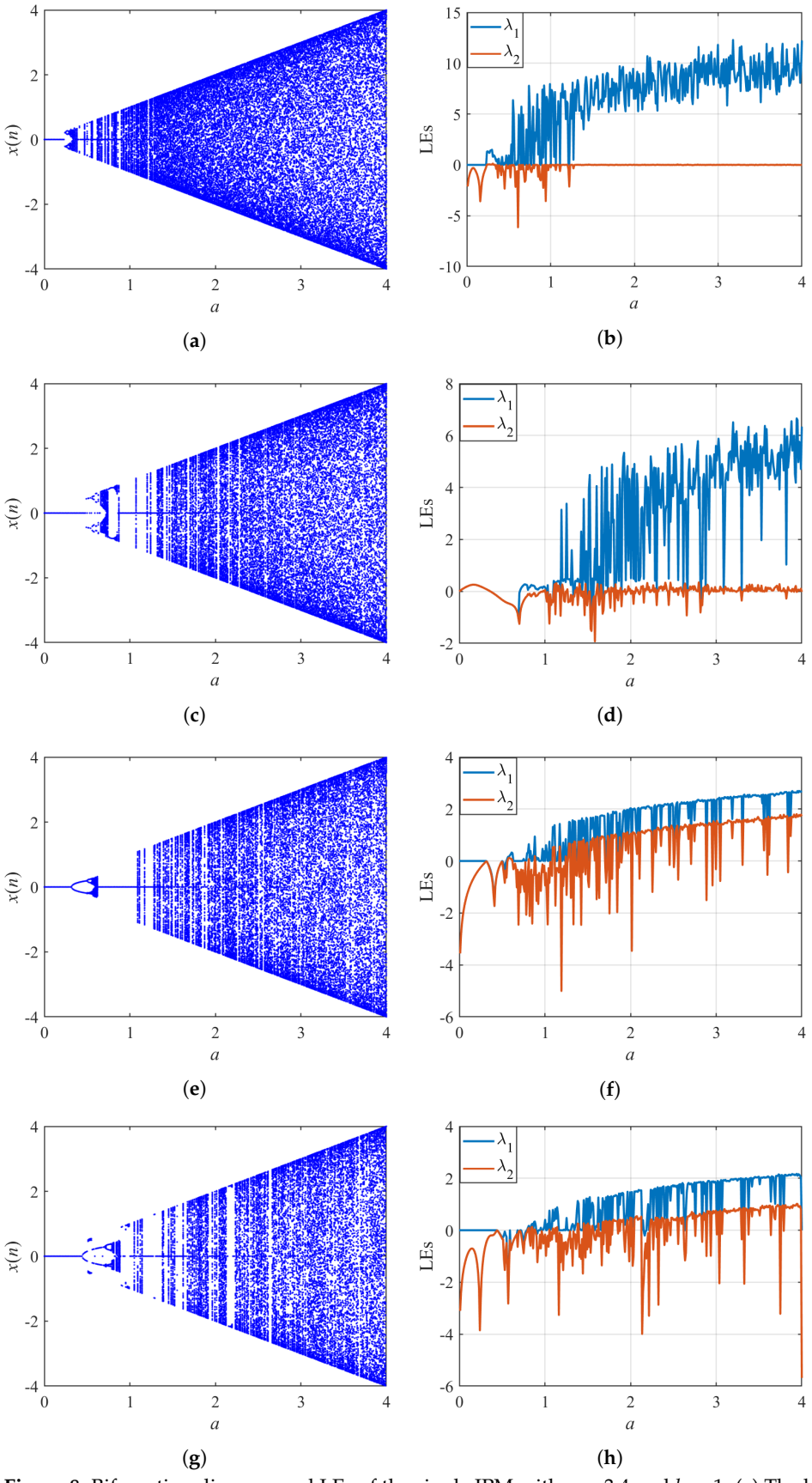


**Figure 8.** Bifurcation diagram and LEs of the single IPM with $a = 3.4$ and $b = 1$. (**a**) The bifurcation diagram of Model 1, (**b**) The LEs of Model 1, (**c**) The bifurcation diagram of Model 2, (**d**) The LEs of

Model 2, (**e**) The bifurcation diagram of Model 3, (**f**) The LEs of Model 3, (**g**) The bifurcation diagram of Model 4, (**h**) The LEs of Model 4.

## 4. Dynamics of Sine Map with Multi-Internal Perturbation

In this section, we analyze the dynamical behaviors of multiple internal perturbation models, which are constructed based on Equation (8), and the block diagram is shown in Figure 5. Three types of discrete memristors are selected (Q-DM, A-DM, and E-DM) because there is a greater impact on the system in the single internal perturbation models. We use these three types of discrete memristors in Equation (8) and Figure 5. Thus, the multiple internal perturbation model of the memristor is constructed as shown in Table 2.

**Table 2.** Multiple internal perturbations of the memristor.

| Model | Memristor | Equation |
|---|---|---|
| Model 5 | Q-DM &A-DM | $\begin{cases} x_{n+1} = a\sin(\omega(x_n - b(q_n^2-1)x_n - b(\lvert q_n\rvert -1)x_n)); \\ q_{n+1} = q_n + x_n \end{cases}$ |
| Model 6 | E-DM& A-DM | $\begin{cases} x_{n+1} = a\sin\left(\omega\left(x_n - b(e^{-\cos(\pi q_n)}-1) - b(\lvert q_n\rvert -1)x_n\right)\right); \\ q_{n+1} = q_n + x_n \end{cases}$ |
| Model 7 | Q-DM& E-DM | $\begin{cases} x_{n+1} = a\sin\left(\omega\left(x_n - b(q_n^2-1)x_n - b(e^{-\cos(\pi q_n)}-1)x_n\right)\right); \\ q_{n+1} = q_n + x_n \end{cases}$ |
| Model 8 | Q-DM, E-DM&A-DM | $\begin{cases} x_{n+1} = a\sin\left(\omega\left(x_n - b(q_n^2-1)x_n - b(e^{-\cos(\pi q_n)}-1)x_n - b(\lvert q_n\rvert -1)x_n\right)\right); \\ q_{n+1} = q_n + x_n \end{cases}$ |

### 4.1. Chaotic Attractor of Multi-Internal Perturbation

Setting the same initial condition as Figure 6, the chaotic attractor diagrams of multiple internal perturbation models are shown in Figure 9. It is obvious that all three models exhibit chaotic behaviors and have better ergodicity compared to Figure 6c,d. This suggests that the perturbations of multiple discrete memristors can enhance the chaotic behavior of the system and increase its complexity. Furthermore, we change $b = 1 \times 10^{-5}$, and the initial condition of the system is consistent with Figure 7. The chaotic attractor diagrams are shown in Figure 10. The results indicate that the ergodicity of the system decreases because parameter $b$ decreases. However, compared with Model 6, Model 5 and Model 7 have more ergodicity and a more complex topology, like Figure 6a. Comparing the equations in Table 2, it was found that both Model 5 and Model 7 contain the Q-DM.

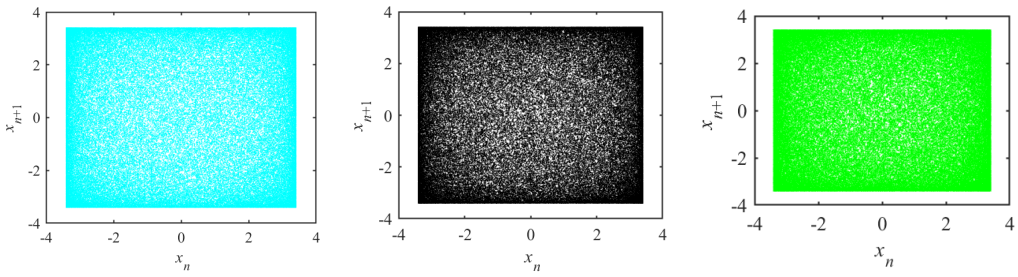


(**a**) (**b**) (**c**)

**Figure 9.** Chaotic attractors with $a = 3.4$ and $b = 1$ (**a**) Model 5, (**b**) Model 6, (**c**) Model 7.

The attractor phase diagram of Model 8, which contains three discrete memristors, is shown in Figure 11. When the parameter $a = 3.4$ and $b = 1$, the corresponding attractor maintains good ergodicity, as shown in Figure 11a. Moreover, when the value of $a$ remains unchanged and $b = 1 \times 10^{-5}$, the chaotic attractor diagram is shown in Figure 11b. As we can see in the figure, the ergodicity of the system and its complexity remain similar to Model 1, Model 5, and Model 7. For models that contain the Q-DM, either single or

multiple perturbations have similar ergodicity. This indicates that the attractor depends on the type of discrete memristor rather than the number of discrete memristors. In Figures 7, 10 and 11, it is revealed that except for parameter $b$, the type of discrete memristor used has a greater impact on improving the ergodicity of the chaotic attractors. Specifically, models that contain the Q-DM have more ergodicity and complex topology. Among the four discrete memristors, the Q-DM appears to be the most effective for improving the ergodicity of chaotic attractors.

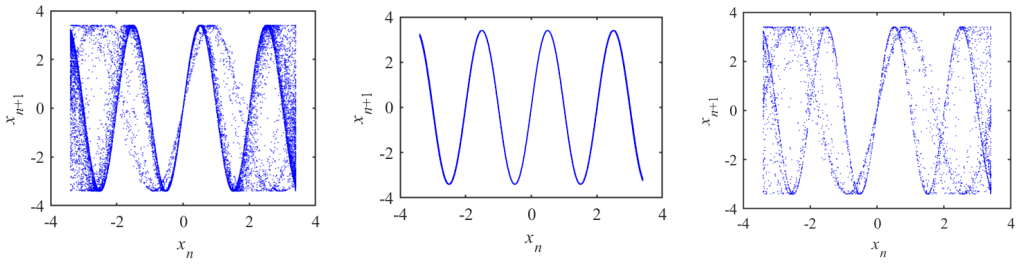


(**a**) (**b**) (**c**)

**Figure 10.** Chaotic attractors with $a = 3.4$ and $b = 1 \times 10^{-5}$ (**a**) Model 5, (**b**) Model 6, (**c**) Model 7.

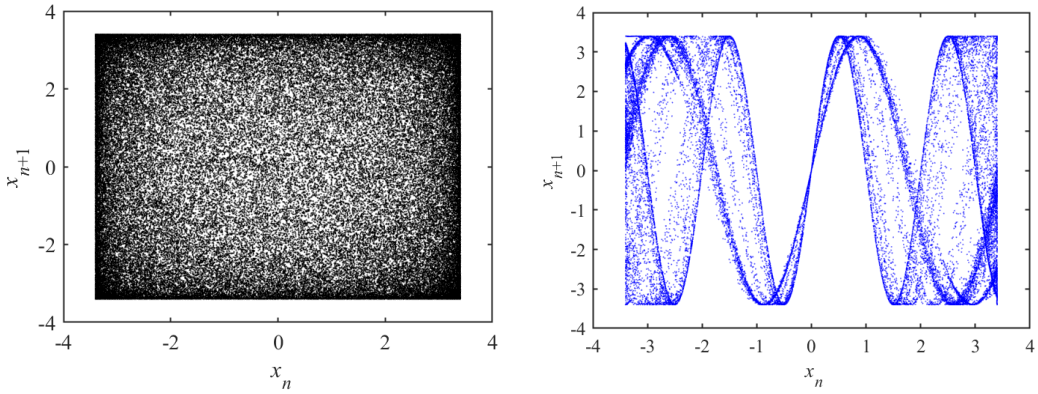


(**a**) (**b**)

**Figure 11.** Chaotic attractor of Model-8 with three memristors (**a**) $a = 3.4$, $b = 1$ (**b**) $a = 3.4$, $b = 1 \times 10^{-5}$.

### *4.2. Bifurcation and LE of Multi-Internal Perturbations*

We analyze the bifurcation and LE of multiple internal perturbation models, which consist of two and three discrete memristors. We set the initial value $x_0 = 0.1, q_0 = 0.2$, a step size of 0.02, and parameters $a = 3.4$ and $b = 1$. The bifurcation diagrams and LEs of Model 5, Model 6, and Model 7 are plotted in Figure 12. The results show that these models exhibit a reduction in period windows compared to the Sine map and Models 1–4. Moreover, the LE values of Model 5 and Model 7 are similar to Model 1 because they all contain the Q-DM. Moreover, the performance of Model 8, which consists of three internal perturbations, is analyzed, and the LEs and bifurcation diagram is shown in Figure 13. The results indicate that the period windows are further reduced by the addition of three discrete memristor perturbations. Meanwhile, the values of the LEs are similar to Model 1, Model 5, and Model 7. From Figures 8, 12 and 13, in the internal perturbation model with multiple memristors, the number of discrete memristors has little effect on the system performance. However, the type of discrete memristor used has a great influence on the system characteristics. From the four discrete memristors, the models containing the Q-DM have the largest LE values.

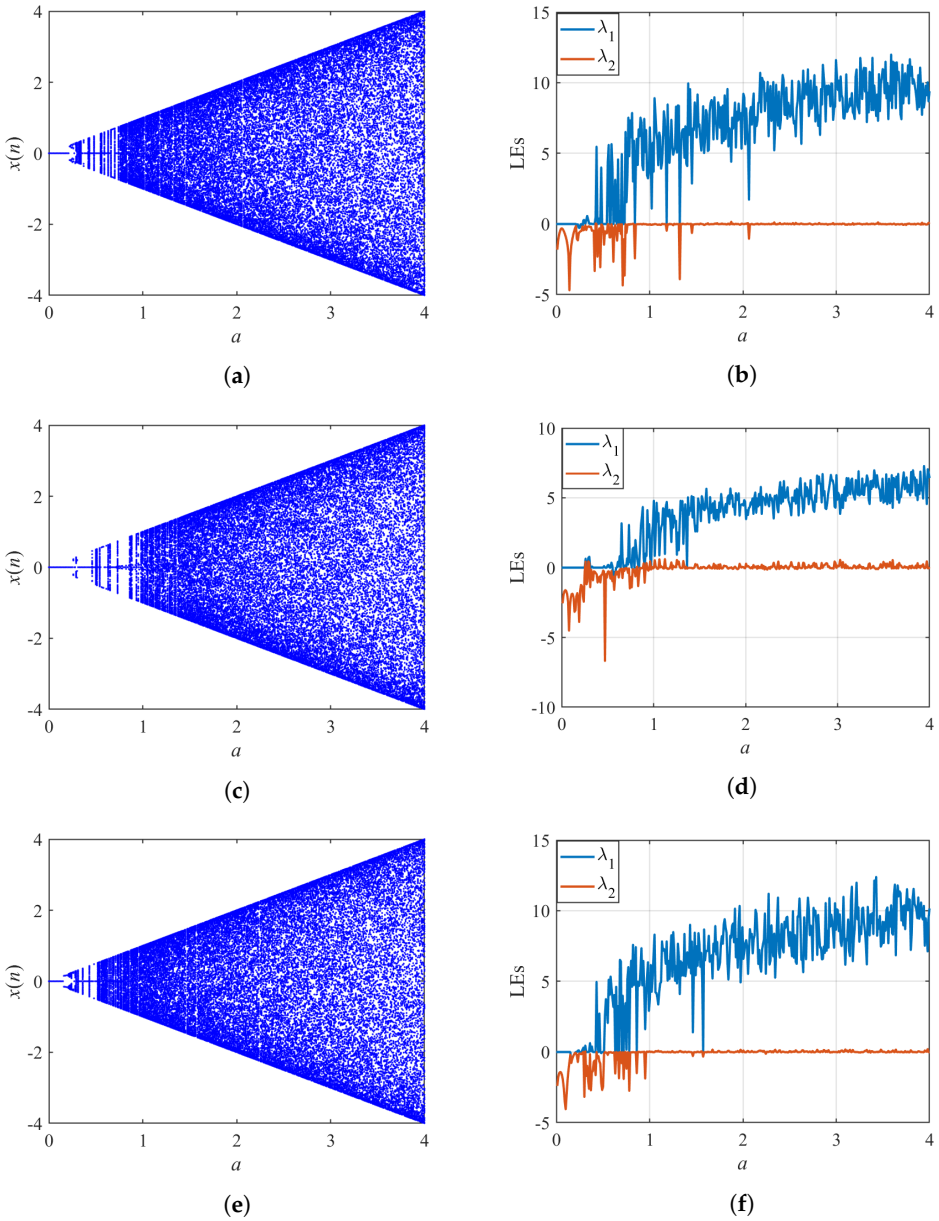


**Figure 12.** Bifurcationdiagrams and LEs of multi-IPM with two discrete memristors. (**a**) The bifurcation diagram of Model 5, (**b**) the LEs of Model 5, (**c**) the bifurcation diagram of Model 6, (**d**) the LEs of Model 6, (**e**) the bifurcation diagram of Model 7, (**f**) the LEs of Model 7.

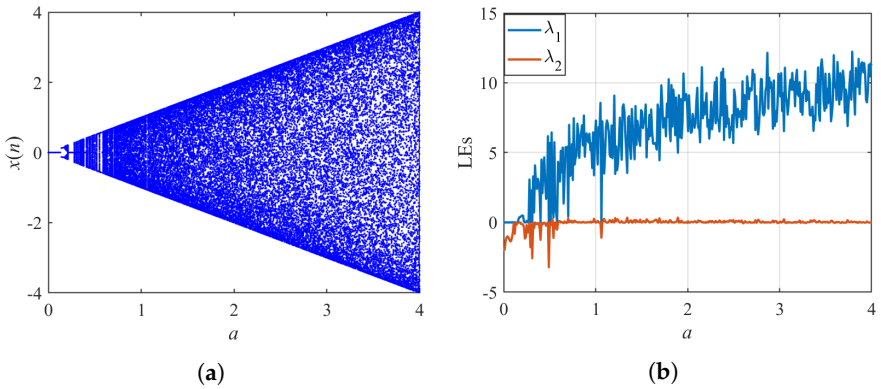


**Figure 13.** Bifurcationdiagrams and LEs of multi-IPM with three discrete memristors, (**a**) the bifurcation diagram of Model 8, (**b**) the LEs of Model 8.

## 5. Pseudo-Random Sequence Generator

Based on the above analysis and comparison, Model 1—with a simpler structure and better performance—is a good choice in practical applications. One of the most important applications of a chaotic map is the pseudo-random sequence generator. It is worth noting that the quantization algorithm is an essential aspect that determines the efficiency of the operation. Therefore, to demonstrate the randomness of chaotic sequences themselves, we choose a simple quantization algorithm, as shown in Equation (9):

$$y = \begin{cases} \lfloor 10^5 \cdot q_n \rfloor \mod 256, & \text{if } q_n > 0; \\ \lfloor 10^6 \cdot q_n \rfloor \mod 256, & \text{if } q_n \leq 0 \end{cases} \tag{9}$$

where $y$ is the pseudo-random sequence generated based on Model 1 and Equation (9). With setting parameters, $a = 3.4, b = 1$, and initial values, $x_0 = 0.1, q_0 = 0.2$, the generated pseudo-random sequence $y$ is tested by NIST. The 100 groups are tested, with each consisting of $10^6$ binary numbers. The test results, listed in Table 3, show that $y$ passes all 15 indicators of NIST SP800-22, indicating that Model 1 with a single discrete memristor perturbation has good chaotic characteristics and complexity.

**Table 3.** NIST test results.

| No. | Test Index | Number of Test | $p$ Value [a] | Proportion | Result |
|---|---|---|---|---|---|
| 1 | Frequency | 1 | 0.304126 | 0.99 | pass |
| 2 | Block frequency | 1 | 0.032923 | 1 | Pass |
| 3 | Cumulative sums | 2 | 0.514124 | 0.98 | Pass |
| 4 | Runs | 1 | 0.798139 | 1 | Pass |
| 5 | Longest test | 1 | 0.779188 | 0.98 | Pass |
| 6 | Rank | 1 | 0.759756 | 1 | Pass |
| 7 | FFT | 1 | 0.383827 | 1 | Pass |
| 8 | Non-overlapping template | 148 | 0.401199 | 0.99 | Pass |
| 9 | Overlapping template | 1 | 0.455937 | 1 | Pass |
| 10 | Universal | 1 | 0.554420 | 0.98 | Pass |
| 11 | Approximate entropy | 1 | 0.236810 | 1 | Pass |
| 12 | Random excursions | 8 | 0.455937 | 0.98 | Pass |
| 13 | Random excursion variant | 18 | 0.534146 | 0.99 | Pass |
| 14 | Serial | 2 | 0.494392 | 0.99 | Pass |
| 15 | Linear complexity | 1 | 0.115387 | 0.98 | Pass |

[a] The results of multiple are averaged.

## 6. Conclusions

This paper proposes a class of chaotic maps by introducing single and multiple discrete memristors as internal perturbations based on the Sine map. We analyze the dynamic behaviors of these models through chaotic attractors, LEs, and bifurcation diagrams. Our numerical simulations demonstrate the discrete memristors as the internal perturbation models of the Sine map not only expand the range of chaos but also significantly improve the LE values and enhance the ergodicity of the system. Additionally, the degree of improvement does not increase significantly with the number of discrete memristors; instead, it depends on the specific type of discrete memristor chosen. As a result, increasing the number of memristors does not always result in a more complex system. In our study with four discrete memristors, we determine that the Q-DM offers the best choice for enhancing the ergodicity of chaotic attractors and improving LEs, providing valuable guidance for designing discrete memristor chaotic systems and emphasizing the importance of selecting the type of memristor used. Furthermore, the pseudo-random sequence generator is designed by utilizing the discrete memristor chaotic map, and the generated sequence is subjected to the National Institute of Standards and Technology (NIST) test.

Next, we will implement the proposed discrete memristor chaotic maps, which have a simple structure and better performance on the hardware platform.

**Author Contributions:** Methodology, S.H.; Formal analysis, S.H. and H.W.; Investigation, W.A.Y. and H.W.; Writing—original draft, W.A.Y.; Writing—review & editing, Z.T. and H.W. All authors have read and agreed to the published version of the manuscript.

**Funding:** This research was supported by the Natural Science Foundation of China (Nos. 62061008, 61901530, 62071496), the Central South University Innovation-Driven Research Programmed (No. 2023CXQD054), and the Natural Science Foundation of Hunan Province (No. 2020JJ5767).

**Conflicts of Interest:** The authors declare no conflict of interest.

## References

1. Chua, L. Memristor–the missing circuit element. *IEEE Trans. Circuit Theory* **1971**, *18*, 507–519. [CrossRef]
2. Chua, L.; Kang, S. Memristive devices and systems. *Proc. IEEE* **1976**, *64*, 209–223. [CrossRef]
3. Strukov, D.B.; Snider, G.S.; Stewart, D.R.; Chua, L. The missing memristor found. *Nature* **2008**, *453*, 80–83. [CrossRef]
4. Adhikari, S.P.; Sah, M.P.; Kim, H.; Chua, L. Three fingerprints of memristor. *IEEE Trans. Circuits Syst. I Regul. Pap.* **2013**, *60*, 3008–3021. [CrossRef]
5. Ilyas, N.; Li, D.; Li, C.; Jiang, X.; Jiang, Y.; Li, W. Analog switching and artificial synaptic behavior of Ag/SiOx: Ag/TiOx/p++-Si memristor device. *Nanoscale Res. Lett.* **2020**, *15*, 30 [CrossRef]
6. Zhang, Y.; Zhuang, J.; Xia, Y.; Bai, Y.; Cao, J.; Gu, L. Fixed-time synchronization of the impulsive memristor-based neural networks. *Commun. Nonlinear Sci. Numer. Simul.* **2019**, *77*, 40–53. [CrossRef]
7. Xu, C.; Wang, C.; Sun, Y.; Hong, Q.; Deng, Q.; Chen, H. Memristor-based neural network circuit with weighted sum simultaneous perturbation training and its applications. *Neurocomputing* **2021**, *462*, 581–590. [CrossRef]
8. Duan, S.; Hu, X.; Dong, Z.; Wang, L.; Mazumder, P. Memristor-based cellular nonlinear/neural network: Design, analysis, and applications. *IEEE Trans. Neural Netw. Learn. Syst.* **2014**, *26*, 1202–1213. [CrossRef]
9. Nagamani, G.; Rajan, G.S.; Zhu, Q. Exponential state estimation for memristor-based discrete-time BAM neural networks with additive delay components. *IEEE Trans. Cybern.* **2019**, *50*, 4281–4292. [CrossRef]
10. Yang, C.; Choi, H.; Park, S.; Sah, M.P.; Kim, H.; Chua, L. A memristor emulator as a replacement of a real memristor. *Semicond. Sci. Technol.* **2014**, *30*, 015007. [CrossRef]
11. Rziga, F.O.; Mbarek, K.; Ghedira, S.; Besbes, K. An efficient Verilog-A memristor model implementation: Simulation and application. *J. Comput. Electron.* **2019**, *18*, 1055–1064. [CrossRef]
12. Gong, L.; Deng, C.; Pan, S.; Zhou, N. Image compression-encryption algorithms by combining hyper-chaotic system with discrete fractional random transform. *Opt. Laser Technol.* **2018**, *103*, 48–58. [CrossRef]
13. Yildirim, M. DNA encoding for RGB image encryption with memristor based neuron model and chaos phenomenon. *Microelectron. J.* **2020**, *104*, 104878. [CrossRef]
14. Luo, J.; Qu, S.; Chen, Y.; Chen, X.; Xiong, Z. Synchronization, circuit and secure communication implementation of a memristor-based hyperchaotic system using single input controller. *Chin. J. Phys.* **2021**, *71*, 403–417. [CrossRef]
15. Caldarola, F.; Pantano, P.; Bilotta, E. Computation of supertrack functions for Chua's oscillator and for Chua's circuit with memristor. *Commun. Nonlinear Sci. Numerical Simul.* **2021**, *94*, 105568. [CrossRef]
16. Lodi, M.; Forti, M.; Storace, M. Stability analysis of the synchronous solution in arrays of memristive Chua's circuits. *IEEE Trans. Circuits Syst. II Express Briefs* **2023**, *70* , 1694–1698. [CrossRef]
17. Kuznetsov, N.; Mokaev, T.; Ponomarenko, V.; Seleznev, E.; Stankevich, N.; Chua, L. Hidden attractors in Chua circuit: Mathematical theory meets physical experiments. *Nonlinear Dyn.* **2023**, *111*, 5859–5887. [CrossRef]
18. Liu, H.; He, P.; Li, G.; Xu, X.; Zhong, H. Multi-directional annular multi-wing chaotic system based on Julia fractals. *Chaos Solitons Fractals* **2022**, *165*, 112799. [CrossRef]
19. Yan, S.; Wang, Q.; Wang, E.; Sun, X.; Song, Z. Multi-scroll fractional-order chaotic system and finite-time synchronization. *Phys. Scr.* **2022**, *97*, 025203. [CrossRef]
20. Lei, T.; Zhou, Y.; Fu, H.; Huang, L.; Zang, H. Multistability dynamics analysis and digital circuit implementation of entanglement-chaos symmetrical memristive system. *Symmetry* **2022** *14*, 2586. [CrossRef]
21. Li, G.; Xu, X.; Zhong, H. A image encryption algorithm based on coexisting multi-attractors in a spherical chaotic system. *Multimed. Tools Appl.* **2022**, *81*, 32005–32031. [CrossRef]
22. Zhong, H.; Li, G. Multi-image encryption algorithm based on wavelet transform and 3D shuffling scrambling. *Multimed. Tools Appl.* **2022**, *81*, 24757–24776. [CrossRef]
23. Yan, D.; Ji, M.; Wang, L.; Duan, S. Memristor-based chaotic system with abundant dynamical behaviors and its application. *Eur. Phys. J. Plus* **2021**, *136*, 1086. [CrossRef]
24. Qi, A.X.; Zhu, B.D.; Wang, G.Y. Complex dynamic behaviors in hyperbolic-type memristor-based cellular neural network. *Chin. Phys. B* **2022**, *31*, 020502. [CrossRef]

25. Xu, B.; Wang, G.; Iu, H.H.C.; Yu, S.; Yuan, F. A memristor–meminductor-based chaotic system with abundant dynamical behaviors. *Nonlinear Dyn.* **2019**, *96*, 765–788. [CrossRef]
26. Yan, W.; Dong, W.; Wang, P.; Wang, Y.; Xing, Y.; Ding, Q. Discrete-time memristor model for enhancing chaotic complexity and application in secure communication. *Entropy* **2022**, *24*, 864. [CrossRef]
27. Zhang, Y.; Liu, Z.; Wu, H.; Chen, S.; Bao, B. Two-memristor-based chaotic system and its extreme multistability reconstitution via dimensionality reduction analysis. *Chaos Solitons Fractals* **2019**, *127*, 354–363. [CrossRef]
28. Ma, J.; Wu, F.; Ren, G.; Tang, J. A class of initials-dependent dynamical systems. *Appl. Math. Comput.* **2017**, *298*, 65–76. [CrossRef]
29. Wang, X.; Gao, M.; Iu, H.H.; Wang, C. Tri-valued memristor-based hyper-chaotic system with hidden and coexistent attractors. *Chaos Solitons Fractals* **2022**, *159*, 112177. [CrossRef]
30. He, S.; Sun, K.; Peng, Y.; Wang, L. Modeling of discrete fracmemristor and its application. *AIP Adv.* **2020**, *10*, 015010. [CrossRef]
31. Peng, Y.; He, S.; Sun, K. A higher dimensional chaotic map with discrete memristor. *AEU-Int. J. Electron. Commun.* **2021**, *129*, 153539. [CrossRef]
32. Liang, Z.; He, S.; Wang, H.; Sun, K. A novel discrete memristive chaotic map. *Eur. Phys. J. Plus* **2022**, *137*, 309. [CrossRef]
33. Liu, T.; Mou, J.; Xiong, L.; Han, X.; Yan, H.; Cao, Y. Hyperchaotic maps of a discrete memristor coupled to trigonometric function. *Phys. Scr.* **2021**, *96*, 125242. [CrossRef]
34. Peng, Y.; He, S.; Sun, K. Chaos in the discrete memristor-based system with fractional-order difference. *Results Phys.* **2021**, *24*, 104106. [CrossRef]
35. Li, G.; Zhong, H.; Xu, W.; Xu, X. Two modified chaotic maps based on discrete memristor model. *Symmetry* **2022**, *14*, 800. [CrossRef]
36. Ma, Y.; Mou, J.; Lu, J.; Banerjee, S.; Cao, Y. A discrete memristor coupled two-dimensional generalized square hyperchaotic maps. *Fractals* **2023**, *11*, 2340136. [CrossRef]
37. Ren, L.; Mou, J.; Banerjee, S.; Zhang, Y. A hyperchaotic map with a new discrete memristor model: Design, dynamical analysis, implementation and application. *Chaos Solitons Fractals* **2023**, *167*, 113024. [CrossRef]
38. Sun, Q.; He, S.; Sun, K.; Wang, H. A novel hyperchaotic map with sine chaotification and discrete memristor. *Chin. Phys. B* **2022**, *31*, 120501. [CrossRef]
39. Hua, Z.; Zhou, B.; Zhou, Y. Sine chaotification model for enhancing chaos and its hardware implementation. *IEEE Trans. Ind. Electron.* **2018**, *66*, 1273–1284. [CrossRef]
40. Li, Y.; He, X.; Zhang, W. The fractional difference form of the sine chaotification model. *Chaos Solitons Fractals* **2020**, *137*, 109774. [CrossRef]
41. Dong, C.; Rajagopal, K.; He, S.; Jafari, S.; Sun, K. Chaotification of Sine-series maps based on the internal perturbation model. *Results Phys.* **2021**, *31*, 105010. [CrossRef]
42. Ramadoss, J.; Ouannas, A.; Tamba, V.K.; Grassi, G.; Momani, S.; Pham, V.T. Constructing non-fixed-point maps with memristors. *Eur. Phys. J. Plus* **2022**, *137*, 211. [CrossRef]
43. Bao, H.; Hua, Z.; Li, H.; Chen, M.; Bao, B. Discrete memristor hyperchaotic maps. *IEEE Trans. Circuits Syst. I Regul. Pap.* **2022**, *68*, 4534–4544. [CrossRef]
44. Bao, H.; Gu, Y.; Xu, Q.; Zhang, X.; Bao, B. Parallel bi-memristor hyperchaotic map with extreme multistability. *Chaos Solitons Fractals* **2022**, *160*, 112273. [CrossRef]
45. He, S.; Zhan, D.; Wang, H.; Sun, K.; Peng, Y. Discrete memristor and discrete memristive systems. *Entropy* **2022**, *24*, 786. [CrossRef]